Iranian Society of Acoustics and Vibration

The 15th ISAV2025 International Conference on Acoustics and Vibration
24-25 Dec 2025 Tehran- Iran

Hygrothermal Stability Analysis of Bio-Inspired Meta-Nanocomposite Shells (ISAV2025)

Farzad Ebrahimi[a*], Mohammadhossein Goudarzfallahi[b], Ali Alinia-ziazi[b]

[a] *Department of Mechanical Engineering, Faculty of Engineering, Imam Khomeini International University, Qazvin, Iran*

[b] *Department of Mechanical and Aerospace Engineering, SR.C., Islamic Azad University, Tehran, Iran*

* *Corresponding author e-mail: febrahimy@eng.ikiu.ac.ir*

Abstract

The present study investigates the effectiveness of a bio-inspired auxetic lattice metamaterial core in enhancing the hygrothermal–torsional stability of carbon nanotube (CNT)-reinforced sandwich cylindrical shells. The shells are subjected to various hygrothermal conditions, including uniform, linear, and nonlinear temperature and moisture gradients. CNTs are embedded within a temperature- and moisture-dependent polymer matrix in the face sheets. The proposed bio-inspired auxetic core, inspired by butterfly wing patterns, exhibits superior adaptability, stiffness, and stability due to its negative Poisson's ratio (NPR), showing improved performance compared to conventional re-entrant type. The equilibrium equations are derived using nonlinear Donnell shell theory with von Kármán geometric nonlinearity and solved via the Galerkin method to obtain buckling and post-buckling responses. The model's accuracy is verified against previous studies. The findings reveal that the butterfly-shaped core achieves up to 23.33% higher stability than the conventional re-entrant core, underscoring its potential for lightweight, high-performance auxetic shell structures. Furthermore, an in-depth parametric analysis is conducted to examine the influence of the hygrothermal environment on the shell's stability behavior.

Keywords: bio-inspired auxetic core; carbon nanotube-reinforced composite; hygrothermal–torsional stability; nonlinear buckling

1. Introduction

Auxetic metamaterials with a negative Poisson's ratio (NPR) have gained increasing attention because of their exceptional mechanical properties, making them ideal, particularly for aerospace, biomedical, and civil applications [1]. Recent developments have led to next-generation auxetic materials with complex architectures beyond conventional re-entrant honeycombs, allowing tailored geometries for enhanced performance. Incorporating such auxetic cores into sandwich composites has shown notable improvements in structural behavior. For instance, Ebrahimi et al. [2] analyzed the stability of toroidal shells with graphene-origami cores. Yu et al. [3] reported that star-shaped auxetic cores enhance the acoustic performance of sandwich plates compared with conventional re-entrant designs. Wang and Fu [4] investigated sandwich plates with bio-inspired auxetic cores.

With the advancement of nanotechnology, carbon nanotubes (CNTs) have emerged as highly effective reinforcements for isotropic matrices, significantly enhancing the thermo-mechanical properties of nanocomposites. Recent studies have extensively examined the stability of CNT-reinforced composite (CNTRC) cylindrical shells under various mechanical and environmental conditions, employing both analytical and numerical approaches. For instance, Shen [5] investigated the post-buckling behavior of CNTRC cylindrical shells in thermal environments. Ly et al. [6] analyzed the stability of CNTRC sandwich shells with honeycomb cores under axial compression, while Dong et al. [7] examined CNTRC sandwich cylindrical shells with auxetic honeycomb cores under torsional loading. More recently, Radwan [8] explored the influence of magnetic fields and hygrothermal conditions on the buckling and vibration behavior of sandwich shells.

The literature review reveals that limited attention has been devoted to auxetic-core CNTRC sandwich cylindrical shells subjected to torsional loading, and existing studies are largely restricted to conventional auxetic geometries and thermal environments alone. In particular, the nonlinear stability and post-buckling behavior of sandwich cylindrical shells incorporating novel bio-inspired auxetic cores under combined torsional loading and hygrothermal fields have not yet been systematically investigated.

To address these gaps, the present study develops a comprehensive nonlinear analytical framework to examine the hygrothermal–torsional stability of CNTRC sandwich cylindrical shells incorporating a bio-inspired butterfly-shaped auxetic core. The formulation is based on Donnell shell theory with von Kármán geometric nonlinearity, and the governing equations are solved using the Galerkin method to determine both buckling and post-buckling responses. The proposed auxetic core is evaluated in comparison with a conventional re-entrant design under various temperature and moisture distributions. Furthermore, an extensive parametric study is performed to clarify the influence of different hygrothermal distribution patterns on the structural performance of the sandwich shells. The results provide new insights into the underlying mechanics governing the stability enhancement of bio-inspired auxetic-core sandwich shells in realistic hygrothermal environments, offering valuable guidance for the design of lightweight, high-performance composite shell structures.

2. Bio-inspired meta-nanocomposite shells

2.1 Geometry and material properties

Fig. 1 illustrates the configuration of a cylindrical sandwich. The structure consists of an auxetic core and CNT-reinforced face sheets, and it is subjected to a uniformly distributed torsional load while being exposed to a hygrothermal environment.

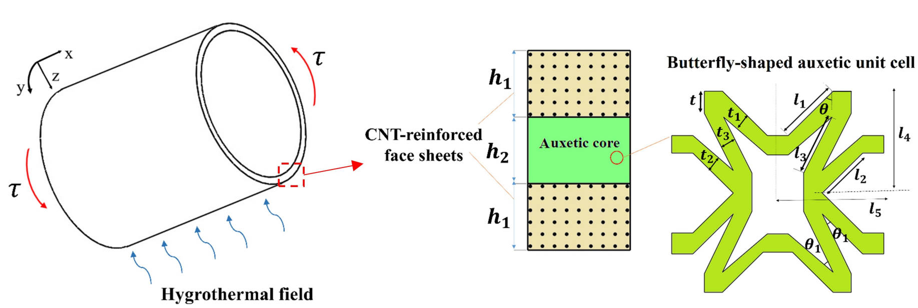

Figure 1. Configuration of the sandwich cylindrical shell under torsional loading and hygrothermal conditions.

The effective elastic moduli of the auxetic layer are provided as follows [4]:

$$E_1^c = \frac{E_s}{\alpha_1[(\mu^3-\mu)\cos^2\alpha + 2 + \mu]} \qquad E_2^c = \frac{E_s\alpha_1}{(\mu^3-\mu)\sin^2\alpha + 2 + \mu}$$
$$G_{12}^c = \frac{E_s l_4 l_5}{2l_4^2\kappa(\cos^2\theta + \kappa^2\sin^2\theta) + r} \quad G_{13}^c = G_{23}^c = G_s\frac{(2\cos\theta + \cos\alpha)^2}{l_4 l_5(2\kappa + \mu)} \tag{1}$$
$$\nu_{12}^c = -\frac{(\mu^3-\mu)\sin(2\alpha)}{2\alpha_1[\mu + 2 + (\mu^3-\mu)\cos^2\alpha]} \quad \nu_{21}^c = -\frac{\alpha_1(\mu^3-\mu)\sin(2\alpha)}{2[(\mu^3-\mu)\sin^2\alpha + \mu + 2+]}$$

The orthotropic elastic constants of CNT-reinforced face sheets are given as [5]:

$$E_{11}^{CNTRC} = V_{ma}E_{ma} + \eta_1 V_{CNT}E_{11}^{CNT}\ ,\ E_{22}^{CNTRC} = \eta_2/\left(\frac{V_{CNT}}{E_{22}^{CNT}} + \frac{V_{ma}}{E_{ma}}\right)$$
$$G_{12}^{CNTRC} = \eta_3/\left(\frac{V_{CNT}}{G_{12}^{CNT}} + \frac{V_{ma}}{G_{ma}}\right),\ \nu_{12}^{CNTRC} = V_{ma}\nu_{ma} + V_{CNT}\nu_{12}^{CNT} \tag{2}$$

2.2 Governing equations

Based on Donnell shell theory and von Kármán nonlinearities, the strain components of the shell are expressed as follows [2]:

$$\begin{bmatrix}\varepsilon_x\\ \varepsilon_y\\ \gamma_{xy}\end{bmatrix} = \begin{bmatrix}\varepsilon_x^0\\ \varepsilon_y^0\\ \gamma_{xy}^0\end{bmatrix} - z\begin{bmatrix}\kappa_x\\ \kappa_y\\ 2\kappa_{xy}\end{bmatrix},\ \begin{bmatrix}\kappa_x\\ \kappa_y\\ \kappa_{xy}\end{bmatrix} = \begin{bmatrix}w_{,xx}\\ w_{,yy}\\ w_{,xy}\end{bmatrix} \tag{3}$$

The nonlinear strain–displacement relations are given as [2]:

$$\varepsilon_x^0 = \frac{\partial u}{\partial x} + \frac{1}{2}\left(\frac{\partial w}{\partial x}\right)^2 \qquad \varepsilon_y^0 = \frac{\partial v}{\partial y} + \frac{1}{2}\left(\frac{\partial w}{\partial y}\right)^2 - \frac{w}{R} \qquad \gamma_{xy}^0 = \frac{\partial u}{\partial y} + \frac{\partial v}{\partial x} + \frac{\partial w}{\partial x}\frac{\partial w}{\partial y} \tag{4}$$

where ε_x^0, ε_y^0, and γ_{xy}^0 are the mid-surface strain components. The deformation compatibility equation derived from Eq. (4) can be written as

$$\frac{\partial^2\varepsilon_x^0}{\partial y^2} + \frac{\partial^2\varepsilon_y^0}{\partial x^2} - \frac{\partial^2\gamma_{xy}^0}{\partial x\partial y} = \frac{\partial^2 w}{\partial x\partial y} - \frac{\partial^2 w}{\partial x^2}\frac{\partial^2 w}{\partial y^2} - \frac{1}{R}\frac{\partial^2 w}{\partial x^2} \tag{5}$$

Hooke's law for the sandwich shell, considering the effects of temperature- and moisture-dependent material properties, is expressed as follows [8]:

$$\begin{bmatrix}\sigma_x\\ \sigma_y\\ \sigma_{xy}\end{bmatrix} = \begin{bmatrix}Q_{11} & Q_{12} & 0\\ Q_{12} & Q_{22} & 0\\ 0 & 0 & Q_{66}\end{bmatrix}\left(\begin{bmatrix}\varepsilon_x\\ \varepsilon_y\\ \gamma_{xy}\end{bmatrix} - (T-T_0)\begin{bmatrix}\alpha_{11}\\ \alpha_{22}\\ 0\end{bmatrix} - (H-H_0)\begin{bmatrix}\beta_{11}\\ \beta_{22}\\ 0\end{bmatrix}\right) \tag{6}$$

With

$$Q_{11} = \frac{E_{11}}{1-\nu_{12}\nu_{21}},\ Q_{12} = \frac{\nu_{21}E_{11}}{1-\nu_{12}\nu_{21}},\ Q_{22} = \frac{E_{22}}{1-\nu_{12}\nu_{21}} \quad Q_{66} = G_{12} \tag{7}$$

where $T - T_0$ and $H - H_0$ are the differences in temperature and moisture, respectively.

By integrating Eq. (6) through the shell thickness, the resultants of the internal forces and moments are expressed as follows:

$$\begin{bmatrix} N_x \\ N_y \\ N_{xy} \\ M_x \\ M_y \\ M_{xy} \end{bmatrix} = \begin{bmatrix} A_{11} & A_{12} & 0 & B_{11} & B_{12} & 0 \\ A_{12} & A_{22} & 0 & B_{12} & B_{22} & 0 \\ 0 & 0 & A_{66} & 0 & 0 & B_{66} \\ B_{11} & B_{12} & 0 & D_{11} & D_{12} & 0 \\ B_{12} & B_{22} & 0 & D_{12} & D_{22} & 0 \\ 0 & 0 & B_{66} & 0 & 0 & D_{66} \end{bmatrix} \begin{bmatrix} \varepsilon_x^0 \\ \varepsilon_y^0 \\ \gamma_{xy}^0 \\ -\chi_x \\ -\chi_y \\ -2\chi_{xy} \end{bmatrix} - \begin{bmatrix} \psi_{1x} \\ \psi_{1y} \\ 0 \\ \psi_{2x} \\ \psi_{2y} \\ 0 \end{bmatrix} \tag{8}$$

where A_{ij}, B_{ij}, and D_{ij} are the components of the stiffness matrix, and ψ_{1x}, ψ_{1y}, ψ_{2x}, and ψ_{2y} denote the thermal and moisture components. The equilibrium equations of the shell can be expressed as follows [7]:

$$\begin{gathered} N_{x,x} + N_{xy,y} = 0 \\ N_{xy,x} + N_{y,y} = 0 \\ M_{x,xx} + 2M_{xy,xy} + M_{y,yy} + N_x w_{,xx} + 2N_{xy} w_{,xy} + N_y w_{,yy} + \frac{N_y}{R} = 0 \end{gathered} \tag{9}$$

The stress function $F(x,y)$ is introduced such that:

$$N_x = F_{,yy}\ ,\ N_y = F_{,xx}\ ,\ ,\ N_{xy} = -F_{,xy} \tag{10}$$

Inserting Eqs. (8) and (10) into the equilibrium equation (9) gives:

$$\begin{gathered} \hat{D}_{11} w_{,xxxx} + (\hat{D}_{12} + \hat{D}_{21} + 4\hat{D}_{66}) w_{,xxyy} + \hat{D}_{22} w_{,yyyy} + \hat{B}_{21} F_{x,xxxx} - (\hat{B}_{11} + \hat{B}_{22} - 2\hat{B}_{66}) F_{,xxyy} - \hat{B}_{12} F_{,yyyy} - \frac{1}{R} F_{,xx} \\ - F_{,yy} w_{,xx} - F_{,xx} w_{,yy} + 2F_{,xy} w_{,xy} = 0 \end{gathered} \tag{11}$$

Inserting Eqs. (8) into Eqs. (5), we obtain:

$$\begin{gathered} \hat{A}_{11} F_{,xxxx} + (\hat{A}_{66} - 2\hat{A}_{12}) F_{,xxyy} + \hat{A}_{22} F_{,yyyy} + \hat{B}_{21} w_{,xxxx} \\ + (\hat{B}_{11} + \hat{B}_{22} - 2\hat{B}_{66}) w_{,xxyy} + \hat{B}_{12} w_{,yyyy} - w_{,xy}^2 + w_{,xx} w_{,yy} + \frac{1}{R} w_{,xx} = 0 \end{gathered} \tag{12}$$

Eqs. (11) and (12) are used to analyze the buckling and post-buckling response of sandwich shells.

3. Solution of governing equations

For simply supported cylindrical shells, the boundary conditions are defined as [7]:

$$w = 0,\ N_x = 0,\ M_x = 0,\ N_{xy} = -\tau h \tag{13}$$

The deflection of the shell is given as follows [7]:

$$w = \xi_0 + \xi_1 \sin\alpha x \sin\beta(y - \lambda x) + \xi_2 \sin^2\alpha x \tag{14}$$

where $\xi_i (i = 1, \ldots, 3)$ are the deflection amplitudes, as described in Dong et al. [7]. Furthermore, the stress function F is obtained by substituting Eq. (14) into Eq. (12), as follows:

$$F = A_1 \cos 2ax + A_2 \cos 2\beta(y-\lambda x) + A_3 \cos\beta\left[x\left(\frac{\alpha}{\beta}-\lambda\right)+y\right] \\ +A_4 \cos\beta\left[y - x\left(\frac{\alpha}{\beta}+\lambda\right)\right] + A_5 \cos\beta\left[y - x\left(\frac{3\alpha}{\beta}+\lambda\right)\right] + A_6 \cos\beta\left[x\left(\frac{3\alpha}{\beta}-\lambda\right)+y\right] - \tau hxy \quad (15)$$

where $A_i(i = 1,\ldots,6)$ are provided in Dong et al. [7]. Substituting Eq. (14) and Eq. (15) into Eq. (11) and applying the Galerkin procedure yields

$$2\tau h\beta^2\lambda + X_1 + X_2\xi_2 + X_3\xi_1^2 + X_4\xi_2^2 = 0 \quad (16)$$

$$-X_6\xi_1^2 + X_5\xi_2 + X_7\xi_1^2\xi_2 = 0 \quad (17)$$

Additionally, applying the closed condition of the shell yields:

$$2\xi_0 + \xi_2 - \frac{1}{4}\beta^2\xi_1^2 R + 2R(\hat{A}_{11}\psi_{1y} - A_{12s}\psi_{1x}) = 0 \quad (18)$$

From Eqs. (16)–(18), the $\tau - \xi_1$ relationship is expressed as:

$$\tau = \frac{-1}{2h\beta^2\lambda}\left[X_1 + \xi_1^2 X_3 + \frac{\xi_1^4 X_4 X_6^2}{(X_5 + \xi_1^2 X_7)^2} + \frac{\xi_1^2 X_2 X_6}{X_5 + \xi_1^2 X_7}\right] \quad (19)$$

As $\xi \to 0$, the upper buckling load is obtained as:

$$\tau^{upper} = \frac{-X_1}{2h\lambda\beta^2} \quad (20)$$

From Eq. (14), the maximum deflection is determined as

$$W_{\max} = \Big\{X_5\big(8\xi_1 + R\beta^2\xi_1^2 + 8\hat{A}_{12}R\psi_{1x} - 8\hat{A}_{11}R\psi_{1y}\big) \\ + \xi_1^2\Big(4X_6 + X_7\big(8\xi_1 + R\beta^2\xi_1^2 + 8\hat{A}_{12}R\phi_{1x} - 8\hat{A}_{11}R\phi_{1y}\big)\Big)\Big\} \\ \times (8(X_5 + X_7\xi_1^2))^{-1} \quad (21)$$

The twist angle ϕ can be determined in the average form as

$$\phi = \frac{1}{2\pi RL}\int_0^{2\pi R}\int_0^{L}\left(\frac{\partial v}{\partial x} + \frac{\partial u}{\partial y}\right)dxdy = \frac{\beta^2\lambda\zeta_1^2}{4} + \tau h\hat{A}_{66} \quad (22)$$

The post-buckling curves are obtained from Eqs. (19) and (21) for the $W_{max}/h - \tau$ response and from Eqs. (19) and (22) for the $\phi - \tau$ response.

4. Numerical results and discussions

The present approach is verified through a comparison of buckling loads of torsionally loaded CNTRC sandwich cylindrical shells with re-entrant honeycomb and solid PMMA core. The validation results, shown in Table 1, confirm the accuracy of this research and agree well with the results reported by Dong et al. [7].

Table 1. Buckling loads τ_{cr} (MPa) of CNTRC sandwich cylindrical shells (m = 1, $T = 300K$).

V_{CNT}	Solid core		Re-entrant honeycomb core	
	Dong et al. [7]	**Present**	**Dong et al. [7]**	**Present**
0.12	31.23	31.5185	22.01	22.2944
0.17	43.53	43.9881	34.37	34.8329
0.28	57.38	57.9493	46.76	47.3329

Table 2 compares the buckling performance of different auxetic cores, including the bio-inspired and re-entrant types. The findings indicate that the proposed bio-inspired core shows consistently higher performance than the re-entrant type for all *R/h* ratios and environmental conditions. For example, at *R/h* = 200 and (ΔT, ΔH) = (50, 0.1), the critical buckling load increases by 20.99%. This improvement further rises to 23.33% at *R/h* = 60 and (ΔT, ΔH) = (100, 0.2). The post-buckling responses shown in Figs. 2(a) and 2(b) further confirm the superior stability of the proposed auxetic core, with higher equilibrium paths over the entire deflection range. This enhanced performance is attributed to the distinctive bio-inspired unit-cell architecture, which promotes more uniform load transfer, increases the effective shear stiffness, and delays the onset of instability, thereby improving both buckling and post-buckling stability.
Table 3 compares the buckling loads for three hygrothermal distribution types—UHD, LHD, and NHD—under various temperature–moisture increments. The results indicate that hygrothermal effects have a significant impact on structural stability. For instance, increasing (ΔT, ΔH) from (50, 0.1) to (250, 0.5) decreases the critical buckling load by 5.08% under NHD, 12.90% under UHD, and 3.91% under LHD. The post-buckling responses ($W_{max}/h - \tau$ and $\phi - \tau$) in Figs. 3a and 3b further confirm this degradation, showing descending post-buckling paths with increasing temperature and moisture. This reduction is primarily because of the softening of the matrix in the face sheets, which decreases the overall stiffness of the composite structure. Among the three distributions, UHD consistently has the most detrimental effect on shell stability, while LHD has the least. The corresponding post-buckling curves in Figs. 4a and 4b show that UHD causes the most significant reduction in load-carrying capacity, whereas LHD and NHD exhibit nearly identical behavior.

Table 2. Buckling loads τ_{cr} (MPa) for torsionally loaded sandwich shells with bio-inspired and re-entrant cores under various temperature/moisture changes (m=1, UHD).

ΔT(K), ΔH(%)	*R/h*	Butterfly-shaped	Re-entrant type	Difference (%)
(50, 0.1)	200	15.5137	12.8227	20.99
	100	33.2405	27.1915	22.25
	80	41.9258	34.9805	19.85
	60	58.8174	48.14	22.18
(100, 0.2)	200	15.0365	12.3713	21.54
	100	32.1794	26.1609	23.01
	80	40.5774	33.7114	20.37
	60	57.0078	46.2255	23.33

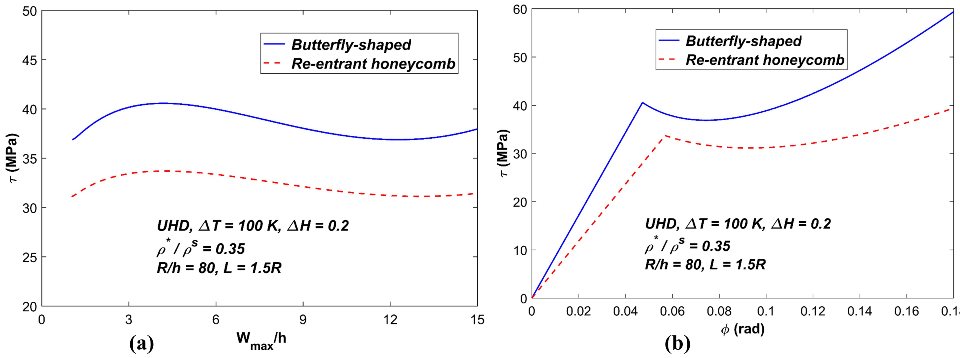

Figure 2. Comparison of post-buckling responses.

Table 3. Buckling loads τ_{cr} (MPa) for torsionally loaded sandwich shells under various hygrothermal distribution types (m=1)

V_{CNT}	ΔT(K), ΔH(%)	UHD	LHD	NHD
	(50, 0.1)	29.5066	30.1695	30.0799
	(100, 0.2)	28.6143	29.9385	29.7608
0.12	(150. 0.3)	27.7275	29.7158	29.451
	(200, 0.4)	26.84	29.4998	29.1481
	(250, 0.5)	25.9453	29.2887	28.8498
	(50, 0.1)	41.9258	42.8403	42.7144
	(100, 0.2)	40.5774	42.4067	42.1568
0.17	(150. 0.3)	39.2329	41.9845	41.6114
	(200, 0.4)	37.8823	41.571	41.0747
	(250, 0.5)	36.5155	41.1636	40.5432

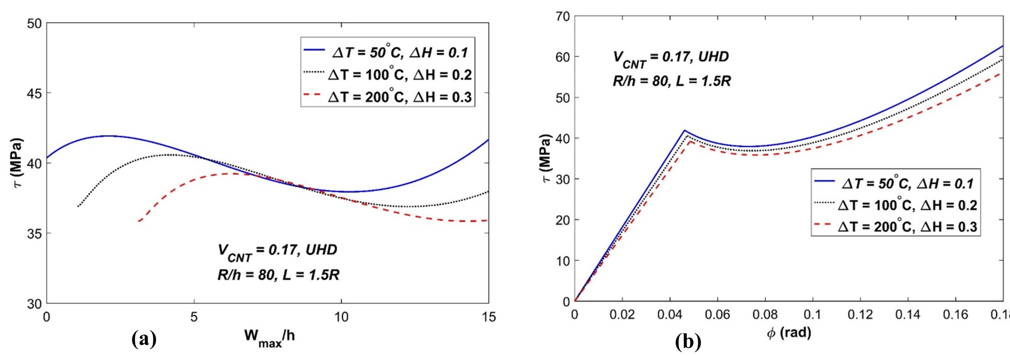

Figure 3. Post-buckling behavior of the sandwich cylindrical shell under increasing temperature and humidity.

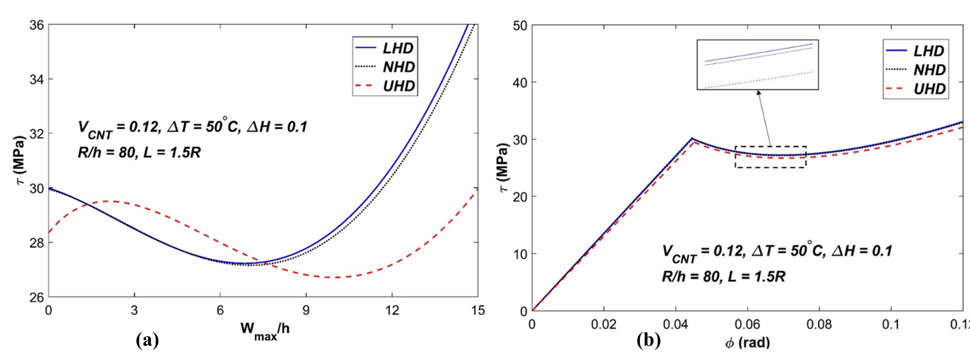

Figure 4. Post-buckling behavior of the sandwich cylindrical shell under various hygrothermal distribution types.

5. Conclusions

This study investigates the nonlinear stability of torsionally loaded nanocomposite sandwich cylindrical shells featuring a bio-inspired auxetic core and CNTRC face sheets in a hygro-thermal environment. The formulations are based on Donnell's shell theory with von Kármán geometric nonlinearity, and the resulting nonlinear equations are solved using the Galerkin method. The main numerical findings are summarized as follows:

The bio-inspired auxetic core outperforms the conventional re-entrant design in torsionally loaded sandwich cylindrical shells under hygrothermal conditions. It consistently yields higher critical buckling loads—up to 23.33% greater—particularly at lower thickness ratios and elevated temperature and humidity levels. Post-buckling analyses further reveal enhanced post-buckling behavior. This improved performance is primarily attributed to the unique unit-cell geometry of the bio-inspired auxetic core, which enables better adaptability under varying geometric and loading conditions, resulting in superior load distribution, stiffness, and overall structural stability. The influence of hygrothermal effects shows that both elevated temperature and increased moisture content significantly degrade the stability of torsionally loaded auxetic-core sandwich cylindrical shells. Among the studied hygrothermal distributions, UHD caused the greatest reduction in critical buckling load (up to 12.90%), followed by NHD (5.08%) and LHD (3.91%). These results underscore the importance of considering hygrothermal distribution in the design of CNT-reinforced composites, as hygrothermal-induced degradation of the face sheet matrix leads to reduced stiffness and diminished overall stability. Future work may extend this framework in several promising directions. Employing higher-order shear deformation theories could improve accuracy for thick shells. Furthermore, investigating dynamic stability, impact response, and coupled multiphysics interactions—such as piezoelectric or electromagnetic effects—would significantly broaden the potential applications of these innovative bio-inspired auxetic-core structures.

REFERENCES

1. F. Ebrahimi, *Mechanics of Auxetic Materials and Structures*, CRC Press, 2024.
2. F. Ebrahimi, M. Goudarzfallahi, A. Alinia Ziazi, "Buckling and postbuckling analysis of graphene origami–enabled auxetic metamaterial sandwich toroidal shell segments subjected to axial compression", *Journal of Engineering Mechanics* **151**, 04025012 (2025).
3. D. Yu, F. Kong, T. Fu, "Sound transmission loss analysis of novel sandwich plate with star-shaped auxetic cellular cores", *Mechanics of Advanced Materials and Structures*, 1–13 (2024)
4. X. Wang, T. Fu, "Improvement of broadband low-frequency sound insulation of sandwich plates with negative Poisson's ratio butterfly-shaped auxetic cellular", *Engineering Analysis with Boundary Elements* **166**, 105852 (2024).
5. H. S. Shen, "Postbuckling of nanotube-reinforced composite cylindrical shells in thermal environments, Part I: Axially loaded shells", *Composite Structures* **93**, 2096–2108 (2011).
6. L. N. Ly, V. M. Duc, N. T. Trung, N. T. Phuong, D. T. Dong, T. Q. Minh, … V. T. Hung, "An analytical approach to the nonlinear buckling behavior of axially compressed auxetic-core cylindrical shells with carbon nanotube-reinforced coatings", *Proceedings of the Institution of Mechanical Engineers, Part L: Journal of Materials: Design and Applications* **235**, 2254–2265 (2021).
7. D. T. Dong, N. T. Phuong, V. H. Nam, L. N. Ly, N. V. Tien, V. M. Duc, … N. T. H. Giang, "An analytical approach for nonlinear buckling analysis of torsionally loaded sandwich carbon nanotube-reinforced cylindrical shells with auxetic core", *Advances in Applied Mathematics and Mechanics* **15**, 468–484 (2023).
8. A. F. Radwan, "Influence of 2D magnetic field and hygrothermal conditions on buckling and vibration of FG sandwich piezoelectric cylindrical shells with a lightweight core embedded in viscoelastic foundations", *Journal of the Brazilian Society of Mechanical Sciences and Engineering* **47**, 94 (2025).